CrossMark

RESEARCH ARTICLE

Flow field interactions between two tandem cyclists

Nathan Barry[1] · David Burton[1] · John Sheridan[1] · Mark Thompson[1] ·
Nicholas A. T. Brown[2]

Abstract Aerodynamic drag is the primary resistive force acting on cyclists at racing speeds. Many events involve cyclists travelling in very close proximity. Previous studies have shown that interactions result in significant drag reductions for inline cyclists. However, the interaction between cyclist leg position (pedalling) and the vortical flow structures that contribute significantly to the drag on an isolated cyclist has not previously been quantified or described for tandem cyclists of varying separation. To this end, scale model cyclists were constructed for testing in a water channel for inline tandem configurations. Particle image velocimetry was used to capture time-averaged velocity fields around two tandem cyclists. Perhaps surprisingly, the wake of a trailing cyclist maintains strong similarity to the characteristic wake of a single cyclist despite a significant disturbance to the upstream flow. Together with streamwise velocity measurements through the wake and upstream of the trailing cyclist, this work supports previous findings, which showed that the trailing cyclist drag reduction is primarily due to upstream sheltering effects reducing the stagnation pressure on forward-facing surfaces.

✉ Nathan Barry
  nathanrbarry@gmail.com

1 Monash University, Clayton, VIC, Australia

2 Australian Institute of Sport (AIS), Belconnen,
  ACT 2617, Australia

1 Introduction

Optimised aerodynamics is paramount to achieving success in competitive cycling. In some events, more than 90% of total energy expenditure by the cyclist is to overcome drag (Kyle and Burke 1984; Grappe et al. 1997). It is well established that drafting (following in the wake of a lead cyclist) offers significant aerodynamic drag reduction for cyclists; however, the flow mechanisms causing this are not well understood. Whilst it is known that a trailing cyclist encounters lower energy flow, it is has not been established how the flow structures in the wake of tandem cyclists are different from an isolated cyclist, and whether these differences contribute significantly to the aerodynamic drag.

There are many engineering applications where two or more bodies are positioned in close proximity in a fluid stream. Cylinders are one of the most studied examples. It has been shown that the flow regime over a cylinder, and consequently the body forces, can be significantly modified by the presence of additional cylinders. Biermann and Herrnstein (1933) found that for tandem cylinders parallel to the flow, both cylinders experience a decrease in drag as a function of separation distance, with the reduction for the trailing cylinder being significantly greater. Two flow regimes that are a function of separation distance have been identified. First, a regime where the flow separating from the lead cylinder reattaches onto the downstream cylinder (low drag). A second, higher drag, regime occurs at greater separation distances as the wake of the lead body closes and a second stagnation point develops on the trailing cylinder (Hori 1959; Ishigai et al. 1972; Zdravkovich 1977; Zdravkovich and Pridden 1977; Lin et al. 2002; Deng et al. 2006).

Springer

The work of Hori ([1959]) and Zdravkovich and Stanhope ([1972]) (discussed in Zdravkovich [1977a]) demonstrates that the pressure on the most forward point of a trailing cylinder decreases due to the presence of an upstream cylinder from a pressure coefficient of approximately $+1.0$ (isolated cylinder) to between approximately -0.9 (1.5 diameters) and 0.0 (7 diameters). Additionally, the base pressure is most negative for the isolated case, meaning that the change in force is attributable to both a reduction in forward surface pressure and an increase in base pressure. The flow conditions experienced by the trailing cylinder, in particular the vorticity field and the incoming turbulence, are modified by the upstream cylinder (Sumner [2010]; Lin et al. [2002]). The trailing cylinder alters the wake dynamics of the upstream cylinder, stabilises the wake and has a drag reducing effect (Lee and Basu [1997]). Interactions between bodies of more complex geometry occur in ground transportation, including passenger, racing and heavy vehicles, as well as in groups of cyclists. The drag force of inline ground vehicles is a strong function of separation distance and geometry (Romberg et al. [1971]; Ioannou [1997]; Hammache et al. [2002]; Watkins and Vino [2008]). The relationship between drag and separation distance varies with the geometry of the vehicle; however, few studies have investigated the flow mechanisms responsible for these effects.

Studies of the aerodynamics of cyclists have typically focussed on the measurement of body forces and correlation of those forces with cyclist position (Zdravkovich et al. [1996]; Grappe et al. [1997]; Gibertini and Grassi [2008]; García-López et al. [2008]). It is only recently that the wake of a cyclist has been characterised. The flow is highly three dimensional and dominated by counter-rotating vortex pairs that vary in strength and location as the leg position changes through the pedalling cycle (Crouch et al. [2012], [2014]; Griffith et al. [2013]). Despite the shape of a cyclist changing through the crank cycle, the wake of a cyclist can be characterised by two key flow regimes: symmetric and asymmetric, which are a function of leg position.

The drag of multiple cyclists has been reported in a number of studies, including Kawamura ([1953]), Kyle ([1979]), Zdravkovich et al. ([1996]), Olds ([1998]), Edwards and Byrnes ([2007]), Torre and Íñiguez ([2009]), Blocken et al. ([2013]), Defraeye et al. ([2014]), Barry et al. ([2014a], [b], [2015]) and Barry ([2016]). These studies all show that the drag of the trailing cyclist is significantly reduced relative to an isolated cyclist and that the drag reduction is highest for the minimum possible spacing. Anthropomorphic characteristics and posture of the cyclists in the group have also been shown to affect the drag reduction experienced (Kyle [1979]; Blocken et al. [2013]; Defraeye et al. [2014]; Barry et al. [2014a], [b]). Kyle ([1979]) applied a coast down method and observed a maximum drag reduction in 39% for the trailing cyclist at the minimum spacing, compared to an earlier scale model wind tunnel study by Kawamura at Tokyo University that found a reduction in 55% (Kawamura [1953]). Barry et al. ([2014a], [b]) conducted full-scale wind tunnel tests of tandem cyclists, using an athlete and a mannequin of similar geometry to the model adopted in this work, and found that the drag of the trailing cyclist is reduced by up to 49% at minimum practical separation—similar to studies by Zdravkovich et al. ([1996]). With cyclists separated by one bicycle length, this effect is degraded; however, the trailing cyclist's drag is still reduced by up to 34% (Kyle [1979]; Barry [2016]).

More recently, Blocken et al. ([2013]) have shown that the lead cyclist's drag is reduced by the presence of the trailing cyclist, much as is seen for other bluff bodies such as cylinders. In a wind tunnel test, Blocken et al. ([2013]) observed a drag reduction in 1.6% for the lead cyclist. This was compared to a set of steady-state RANS simulations of cyclists, without bicycles, which found drag reductions in up to 2.6%. A slightly larger drag reduction was seen in experiments by Barry et al. ([2014a], [b]) for the lead cyclist, who found a maximum drag reduction in 5%. Whilst the drag reduction in the lead cyclist is less than the trailing cyclists, it is nevertheless an important finding, as the pace of the team is set by the lead cyclist. A similar, but more pronounced effect on the lead cyclist drag has been observed in the case of a trailing motorcycle with a drag reduction in up to 8.7% for a single motorcyclist (Blocken et al. [2016]), highlighting that the size of the trailing body contributes to the magnitude of this effect.

Blocken et al. ([2013]) performed RANS simulations of tandem cyclists with legs in an approximately symmetrical orientation, without modelling bicycles, and provided insights into the resulting flow field in the form of static pressure profiles. The presence of the trailing cyclist close to the leader indicated an increase in the static pressure towards the rear of the leader, accounting for the leader's drag reduction. These results also showed distortion of the static pressure field around the trailing cyclist, but the flow onto the lead cyclist was unaffected. The authors argued that the reduction in drag of the trailing cyclist was caused by two factors: a decrease in pressure on the front of the trailing cyclist and a decrease in absolute underpressure (i.e. an increase in the base pressure) behind the trailing cyclist.

Blocken et al.'s ([2013]) work suggests that there is some change in strength, nature and distribution of flow structures behind the trailing cyclist. This raises the question of how the changes in drag or pressure distribution observed for tandem cyclists are associated with specific changes to the flow structures described by Crouch et al. ([2014]). In particular, it is not known whether the characteristic symmetric and asymmetric flow regimes seen in that work on a single cyclist also exist behind cyclists in tandem formation.

The complex wake of a cyclist and the existence of two distinctive flow regimes make the flow interactions between multiple cyclists a particularly interesting case study. To that end particle image velocimetry (PIV) was used to interrogate the wake of scale model tandem cyclists in a water channel. The changes to the wake of a trailing cyclist caused by the presence of an upstream cyclist and how these vary with cyclist separation distance was investigated. In particular, the aim was to identify the flow mechanisms that cause the drag changes and determine whether the characteristic wake structures (symmetric and asymmetric) of a single cyclist persist in the wake of a trailing cyclist in a tandem pair.

2 Methodology

Scale models of a cyclist were manufactured at one-seventh of full scale and tested in the Monash University *FLAIR* recirculating water channel. The water channel working section dimensions are: width 600 mm, depth 800 mm, and test section length 4000 mm. The turbulence intensity of the channel was characterised by Venning et al. (2015) and is <0.5% with non-uniformity of ±1% outside the boundary layer. All tests were conducted at a water velocity of 0.38 m/s corresponding to a Reynolds number of approximately 33,000. The characteristic length is defined as the torso chord length, and the length of the cyclist from shoulder to hip ($C = 86$ mm for model and 600 mm for a full-scale cyclist). The Reynolds number is more than an order of magnitude lower than the full-scale conditions that it attempts to predict (approximately 520,000 at 50 km/h). However, since the dominant structures of interest in the cyclist wake are caused by pronounced anthropomorphic features (such as leg position), the authors propose that these will be present at the lower Reynolds number of these tests. The scale model geometry is a simplification of the full-scale mannequin studied by Crouch et al. (2012, 2014, 2016) and Barry et al. (2014a, b); therefore, the results of this study are compared to those experiments.

Each scale model is a rapid-prototyped three dimensionally solid body with fixed leg position. Crouch et al. (2014, 2016) have previously shown that the characteristic flow regimes observed for a static cyclist are consistent with snapshots from the dynamic wake of a pedalling cyclist. Three separate models were fabricated: two at a crank angle of 15°, which we term the *symmetric* condition, and one at a 75° crank angle, which we term the *asymmetric* condition. These are shown in Fig. 1. In the asymmetric condition, the cyclist's left thigh is near its highest point. However, in any test a maximum of two cyclists were used, meaning that the configurations of
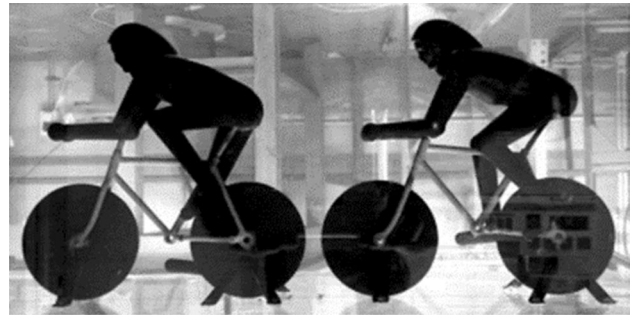

Fig. 1 Photograph of models in the asymmetric–symmetric leg position at Spacing 1 (inverted to actual mounting)

symmetric–symmetric (lead-trailing), symmetric–asymmetric and asymmetric–symmetric conditions could be investigated. Whilst the bicycle contributes to approximately 20–30% of total drag (Kyle and Burke 1984; Crouch et al. 2014), the flow structures of interest here are generated over the back and from the hips. For this reason, and ease of manufacture, we have adopted simplified bicycle models. The bicycles have disc wheels and a tubular frame without handlebars, chains, cranks, pedals or saddles. Each bicycle has a pair of thin blade struts fixed to the rear wheel axle and a single supporting pair attached to the front wheel to hold the model.

The models were mounted to an inverted artificial ground plane suspended in the centre of the test section to minimise wall and free-surface interference. A diagram of the set-up and imaging used is shown in Fig. 2. The length of ground plane was 1200 mm and extended the full width of the water channel. The ground plane extended 1 bicycle length (front wheel leading edge to rear wheel trailing edge, $L = 2.67$ and $C = 230$ mm) upstream of lead cyclist, equivalent to 1700 mm at full scale, and a minimum of $1.4L$ downstream of trailing cyclist. The leading edge had an elliptical profile and resulted in a boundary layer height of $0.06H$ (top of helmet height, $H = 216$ mm) at the front wheel of the first cyclist. Blockage was <1% of the channel cross section.

Single cyclist PIV data were collected for both the symmetric and asymmetric cases. For the tandem formation, both cyclists were laterally aligned and measurements were taken for two cyclist separation distances, *Spacing 1* and *Spacing 2*, see Fig. 3. Spacing 1 was equivalent to 150-mm full scale ($0.25C$), an estimate of the minimum practical spacing, measured from the trailing edge of the lead cyclist rear wheel to the leading edge of the trailing cyclist's front wheel. Spacing 2 had one bicycle length ($2.83C$) between the leading and trailing cyclists. Considering the gap between the bodies of the cyclists, at Spacing 1 the effective spacing is $1.42C$ from the rear of the leader to the head of the trailing cycling and for Spacing 2 it is $4.25C$.
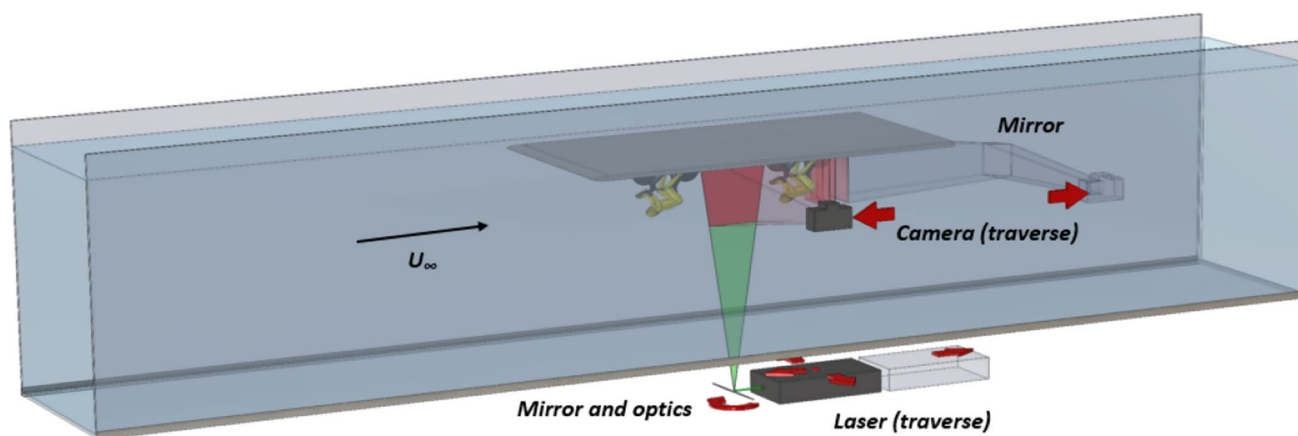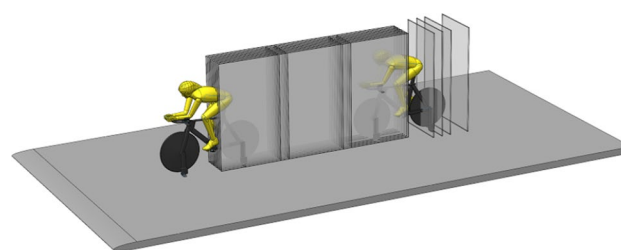
Fig. 2 Schematic of experimental configuration showing traversable camera and laser, mirrors and optics
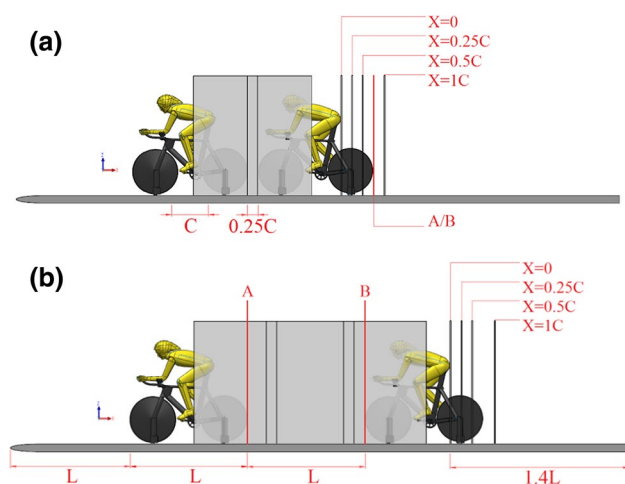
Fig. 3 Profile view of set-up at the two tandem positions: Spacing 1 (*top*) and Spacing 2 (*bottom*). Location of wake cross-sectional planes is also depicted behind the trailing cyclist

Fig. 4 Key PIV imaging planes shown for Spacing 2. 9 lateral planes shown for capturing flow between cyclists

allowing for structures of larger than $0.03C$ (~3 mm) to be identified. This is sufficiently small to identify the main flow structures (hip, thigh and knee vortices) that are of interest in this work.

Each velocity profile was generated from the mean of at least 360 image pairs, taken at 1 Hz, to provide a stable average. The image dimensions were approximately 240 mm (2.8C) high and 150 mm (1.8C) wide. Convergence of mean velocity components was typically found within 200 snapshots. Standard deviation of the cross-stream velocity components from individual PIV snapshots, averaged over the entire field, was 8% of the freestream. The system has a particle image displacement accuracy of approximately 0.1 pixels, which translates to a typical displacement uncertainty of approximately 1%. Other biasing effects exist include those related to laser thickness, particle location within interrogation windows (and therefore true vector position), and tracer particle flow path which contribute to inaccuracies in these results. Accounting for these factors, the overall uncertainty in the velocity measurements is estimated to be the order of $\pm 2\%$, which is a similar order accuracy to that identified in the review of Westerweel et al. (2013) for state-of-the art planar PIV systems. The method adopted for calculation of

A single-camera set-up captured two-dimensional in-plane velocity components in the cross-sectional planes (Fig. 2). The flow was seeded with hollow microspheres with a nominal diameter of 56 μm and a density of 1.016 g cm^{-3} (Vestosint, Germany). Two miniature Nd:YAG pulsed lasers (Minilite II Q-switched lasers, Continuum) that emit light at a wavelength of 532 nm and energy of 25 mJ per pulse were used to produce the laser sheets for illumination of the particles. A charge-coupled camera was used to capture the PIV image pairs (PCO 2000 or 4000). Velocity vectors were computed by cross-correlating image pairs using in-house software applied to 32-by-32 pixel interrogation windows with 50% window overlap (Fouras et al. 2008). These windows correspond to a vector grid spacing of approximately 0.01C (<1 mm),

vorticity follows that outlined in Fouras and Soria (1998), which provides an evaluation of the accuracy of out-of-plane vorticity measurements derived from in-plane velocity field data.

To characterise the near-wake structures behind the trailing cyclist, mean velocity-field projections were obtained in three Y–Z cross-sectional planes (Figs. 3, 4) at $x = 0.25$, 0.5 and $1C$ downstream from the rear of the cyclist torso ($x = 0$). An X–Z image plane through the centre of the cyclist(s) was used to determine streamwise (U) and vertical (W) velocity components. To maintain spatial resolution, multiple image frames were joined to generate the projected centre-plane time-mean velocity field over the entire streamwise domain length. Adjacent image frames were overlapped by a maximum of $0.64C$ (35 mm). In this region, the mean of the two frames was calculated.

A composite technique was used to investigate the mean streamwise flow between the leading and trailing cyclists; this was necessary because the presence of the cyclists obscures part of the imaging plane from the camera. A series of nine X–Z planes were captured at $0.12C$ (10 mm) intervals laterally; these planes are shown in Fig. 4. These were focussed on the region between the two cyclists. The streamwise velocity data from these nine planes, as shown in Fig. 4, were interpolated in the y-direction to generate wake cross sections of the streamwise velocity field. These profiles were only captured for the symmetric–symmetric tandem configuration.

3 Single cyclist wake structure

The streamwise vorticity fields (s^{-1}) in the Y–Z plane obtained from full-scale wind tunnel tests by Crouch et al. (2014) at $x = 0.5$ and $1.0C$ are shown in Fig. 5 alongside those obtained in this study at $x = 0.25$ and $0.5C$. In each case, the vortex boundaries have been identified using the swirling strength criterion, which identifies vortex boundaries from the eigenvalues of the velocity gradient tensor (Zhou et al. 1999). Both sets of results have a symmetric vorticity distribution about the centreline ($y = 0$). The upper hip vortex pair and inner thigh vortex pair are evident in the near body planes ($x = 0.25$ and $0.5C$). However, at the $x = 1C$ plane the coherent structures, evident as concentrated regions of vorticity, have largely diffused. The scale results show the individual vortices diffusing more rapidly as they convect downstream. Results from this study are presented at $x = 0.25C$ (not available at full scale) as this cross section is most similar to full-scale results at $0.5C$, further supporting the more rapid diffusion at the lower Reynolds number. At $x = 1C$ downstream, the vorticity distributions are similar (supplementary online material Figure S1), with both showing broad regions of counter-rotating vorticity.

In the asymmetric condition, the scale model produces the expected clear asymmetry in the left and right hip vortices (see Fig. 6), similar to the full-scale mannequin results of Crouch et al. (2014). However, the strong diagonal flow from the top left of the cyclist to the lower right is less pronounced in downstream planes. This appears to be a result

Fig. 5 **a** Wind tunnel results of Crouch et al. (2014) showing streamwise vorticity (s^{-1}) in the wake of a full-scale cycling mannequin at the symmetric leg position at $0.5C$ downstream of rear of cyclist and **b** $1.0C$ downstream. **c** Vorticity in the wake of scale model cyclist at the symmetric leg position at $0.25C$ downstream of the rear of the cyclist, and **d** $0.5C$ downstream. Contours of swirling strength criterion identify vortex boundaries as used by Crouch et al. (2014)
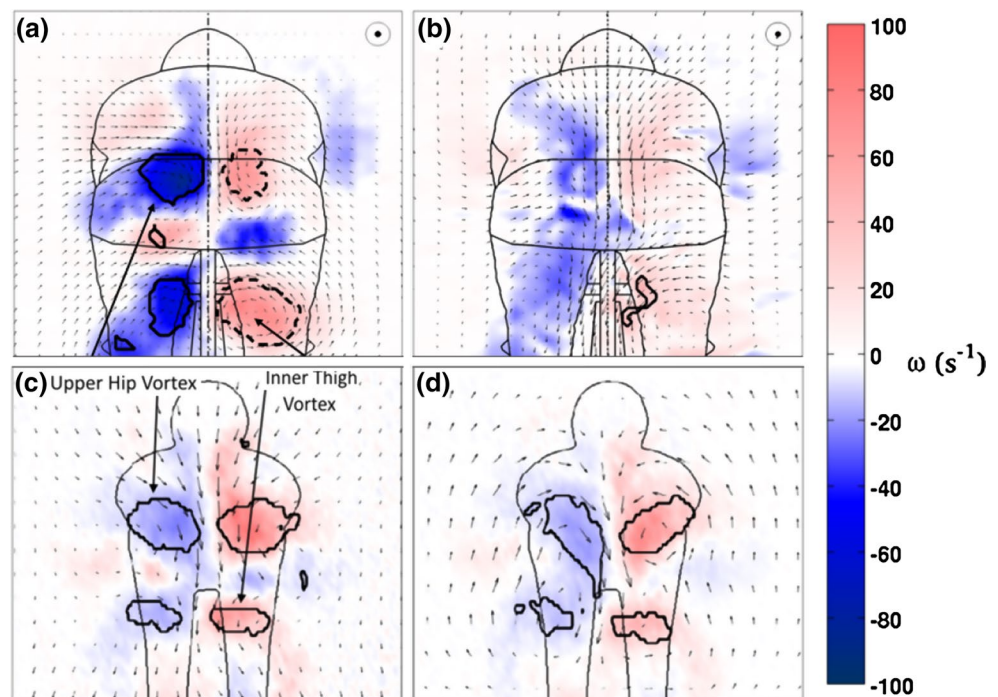
Fig. 6 **a** Wind tunnel results of Crouch et al. (2014) showing streamwise vorticity (s^{-1}) in the wake of a full-scale cycling mannequin at the asymmetric leg position at 0.5C downstream of cyclist, **b** 1.0C downstream. **c** Vorticity in the wake of scale model cyclist at the asymmetric leg position at 0.25C downstream of the rear of the cyclist, and **d** 0.5C downstream. Contours of swirling strength criterion identify vortex boundaries, as used by Crouch et al. (2014)
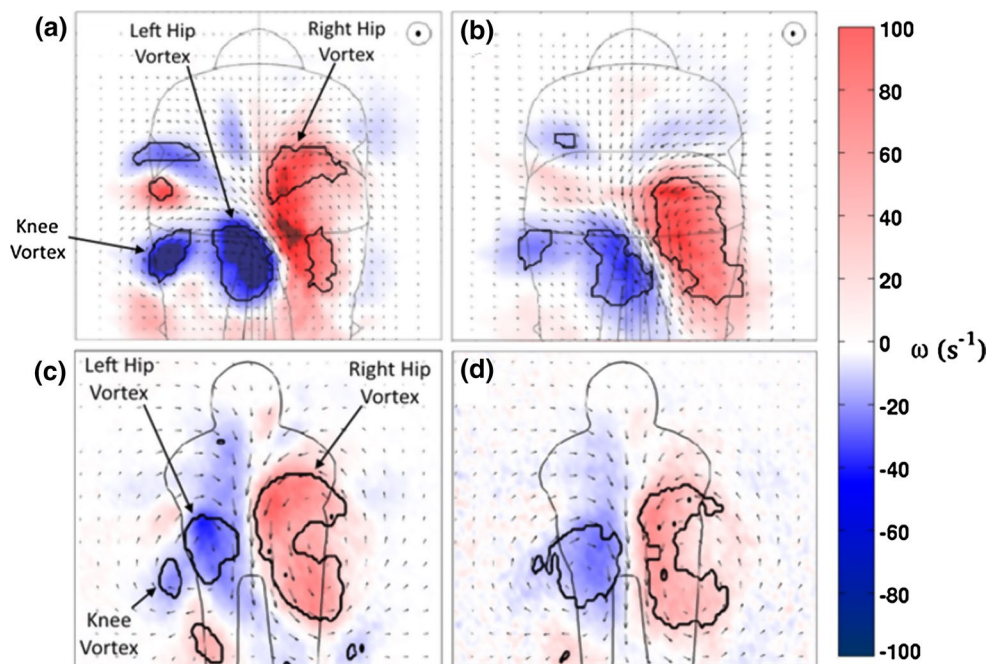
of the left hip vortex being higher and further from the centre, which reduces the interaction with the right hip vortex. The position of this vortex is likely influenced by slight geometric nuances between the two cyclist models changing the interaction between the flow over the hip and back. It may also be linked to the difference in Reynolds number changing the flow separation over the left hip. A smaller knee vortex is also evident at $x = 0.25C$, positioned wide of the left hip vortex, but this diffuses further downstream.

As found in the symmetric case, the structures diffuse at a higher rate in the scale experiment. At $x = 1C$, the full-scale results continue to exhibit a high degree of asymmetry, whereas the scale model results begin to lose the cross-flow component behind the hips at $x = 0.5C$. By $x = 1C$, the asymmetry between the counter-rotating hip vortices is further degraded and the asymmetry in the wake structure no longer prominent (supplementary online material Figure S2). Whilst the relative position of the left and right vortex may influence this result, it is suspected that there is a Reynolds number effect.

The dominant flow structures, in particular the hip vortices, for both symmetric and asymmetric wakes identified in the work of Crouch et al. (2014) are also present in these lower Reynolds number experiments. It follows then, with appropriate regard to the higher diffusion rate, that studying the wake of a trailing cyclist at this Reynolds number will provide insight into whether the main flow structures are similar or distinct from those of a single cyclist. Of concern is the higher rate of diffusion of these structures at the lower Reynolds number. The interaction between the flow structures in the wake of the lead cyclist and the body of

the trailing cyclist will likely be less in these experiments than in full scale, suggesting that these results are more indicative of greater spacing at full scale.

4 Streamwise vorticity in the wake of tandem cyclists

Streamwise vorticity in the wake of the trailing cyclist for the symmetric–symmetric, asymmetric–symmetric, and symmetric–asymmetric cases is presented and discussed in this section. In all cases, the plane $X = 0.25C$ downstream of the trailing cyclist is presented. All vorticity results are non-dimensional: calculated from freestream velocity and position (normalised by cyclist chord length). These results are presented in Fig. 7 together with the single cyclist cases for comparison.

4.1 Symmetric–symmetric condition

Contours of streamwise vorticity behind the trailing cyclist at Spacing 1 and Spacing 2 in the symmetric–symmetric case are shown in Fig. 7c, d. At Spacing 1, the pair of upper hip vortices, seen for a single cyclist, remain the dominant feature in the wake, although vorticity is decreased. Peak vorticity is reduced by a maximum of 28% in the hip vortices. A broad reduction in vorticity is observed across the wake region; likely, the result of the reduced energy in the inlet flow is seen by the trailing cyclist. The inner thigh vortices have reduced in vorticity magnitude and shifted downwards and outwards from the cyclist centreline compared
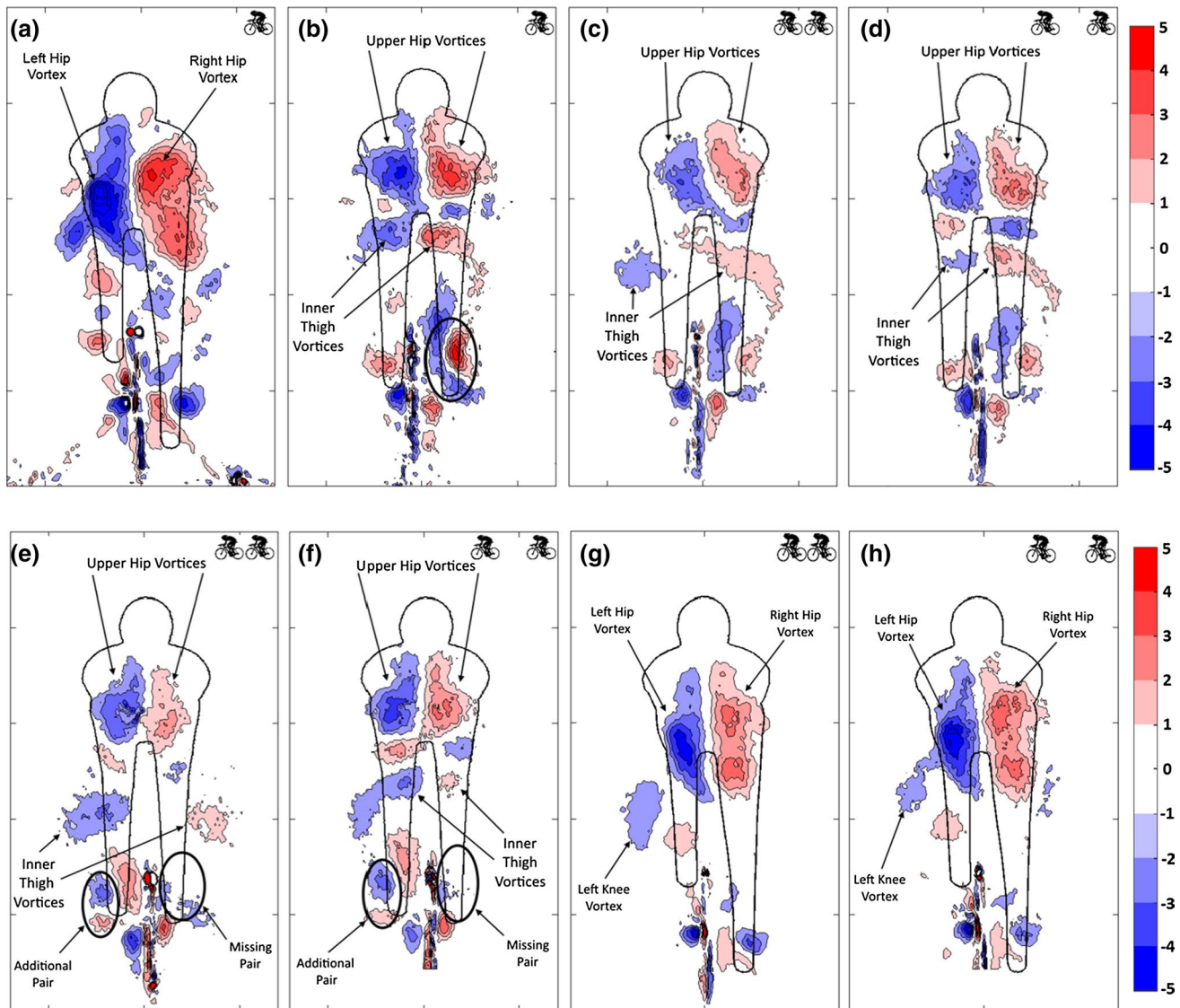
Fig. 7 Streamwise vorticity (non-dimensional) at **a** $x = 0.25C$ downstream of: **a** single cyclist asymmetric case, **b** single cyclist symmetric case, **c** trailing cyclist at Spacing 1 symmetric–symmetric case, **d** trailing cyclist at Spacing 2 symmetric–symmetric case, **e** trailing cyclist at Spacing 1 asymmetric–symmetric case, **f** trailing cyclist at Spacing 2 asymmetric–symmetric case, **g** trailing cyclist at Spacing 1 symmetric–asymmetric case, and **h** trailing cyclist at Spacing 2 symmetric–asymmetric case

to the single cyclist result. There is a localised change in spanwise velocity immediately below the cyclist's hips. This indicates a change in the local in-plane velocity gradient, which is why the vortices are seen lower and wider in the wake. This change in velocity is likely due to the flow coming through the trailing cyclist's legs. Thigh vortices are formed from the inside of the cyclist's legs and so their formation will be affected by the changed flow conditions due to the lead cyclist wake. In the trailing cyclist case, the flow between the legs will contain vorticity and cross-flow velocity components as well as reduction in streamwise velocity due to the presence of the leading cyclist. The combined effect of these flow changes on the formation and evolution

of the thigh vortices contributes to the changes observed in the inner thigh vortices. Secondary features in the lower part of the wake are consistent with the single cyclist profile, but with a reduction in vorticity evident.

For Spacing 2 (Fig. 7d), the wake profile of the trailing cyclist exhibits closely matches that of the single cyclist. Three stacked pairs of counter-rotating vortices behind the torso are clearly evident in the trailing cyclist wake. The upper hip vortices and inner thigh vortices occur in the same relative position as seen for a single cyclist, although magnitude of vorticity is slightly reduced. No combining of vorticity regions across the centreline is evident, as was seen for Spacing 1. Secondary features in the lower region

of the wake are consistent with the single cyclist profile and the vorticity reduction across the wake. However, in downstream planes the thigh vortices diffuse rather than combine with the hip vortices. At Spacing 1, the wake is not symmetric, demonstrating a different wake profile to the single cyclist case, but by Spacing 2 the primary features of the wakes are the same.

Additional planes of vorticity (at $X = 0.5$–$1.0C$) are provided in Figure S3 of the supplementary online material that show the structures identified at $X = 0.25C$ for each case gradually diffusing downstream.

4.2 Asymmetric–symmetric condition

This case provides insight into the effect of an upstream asymmetric wake on the wake of the more symmetric body. At Spacing 1 (Fig. 7e), the three stacked pairs of trailing vortices are apparent and the upper hip vortices are the dominant feature of the wake as was seen for single and symmetric–symmetric cases. However, as with the previous case, peak vorticity is reduced, in this case by 23 and 36% for left and right hip vortices, respectively. On average, this reduction is very similar to that seen in the symmetric–symmetric condition. The bias to the left is likely due to the lead cyclist wake, which has significantly higher vorticity in the left hip vortex compared to the right (-8 and 5.5, respectively). Some persistence of this vorticity into the trailing wake appears to result in greater negative vorticity in the left hip vortex relative to the right. The asymmetric condition has higher peak vorticity and the vortices persist further downstream compared to the symmetric condition; thus, there is a greater influence from the leader wake. The inner thigh vortices are displaced significantly downwards and outwards from the rear of the cyclist, similar to the symmetric–symmetric case. However, in difference, there is no combining of vortices across the centreline. The slight bias to the left side inner thigh vortex is likely the result of vorticity persisting from the leader wake.

Figure 7b shows a strong counter-rotating vortex pair behind the right foot/lower leg for the single cyclist case. However, the pair are absent from the trailing cyclist profiles. These were visible in the symmetric–symmetric case, indicating some dependence on the leader wake profile. Considering the single cyclist asymmetric profile, there is a distinct negative vortex on the outside of the right lower leg/foot, whereas at the corresponding location in the symmetric case the vortex is of positive sign. The positive vorticity generated at the wheel hub also differs in the asymmetric case. It seems then that the vorticity generated from the leading cyclist is impacting on the trailing cyclist right leg and cross-annihilating to eliminate that positive vortex. This is disrupting the formation of that counter-rotating pair observed in the single cyclist symmetric case.

On the left side, there is a small additional counter-rotating vortex pair in the trailing cyclist profiles. These were not evident in the single cyclist wake. Whilst they do not appear to correlate directly with structures in the single asymmetric condition, that region of the wake is characterised by small pockets of vorticity, rather than strong coherent structures. Therefore, it is believed that the interaction of this flow on the right leg of the trailing cyclist is altering the nature of the flow separation, resulting in the small additional counter-rotating pair.

At Spacing 2, the three paired vorticity regions in the upper wake are clearly visible, as seen for the previous symmetric–symmetric case. The upper hip vortices remain the dominant feature of the wake but with a reduction in peak vorticity; 12% left, 21% right. This bias appears to be linked to the bias in vorticity in the leading cyclist wake, as described above, despite the separation distance. The inner thigh vortices remain close to the cyclist centreline compared to Spacing 1, similar to the symmetric–symmetric case. These vortices also show significantly lower vorticity compared to the single cyclist case. The vortex pair on the lower right that was missing in the Spacing 1 wake is also absent at Spacing 2. The additional vortex pair on the lower left is again evident. This was not so in the symmetric–symmetric case, indicating that this pair has its origins in the leading cyclist's wake. Despite the increase in separation distance, the wake of the leader still has an impact on the flow from the lower legs of the trailing cyclist.

The distribution of the thigh vortices of the asymmetric–symmetric case at Spacing 2 appears to be a mirror of the behaviour seen in the symmetric–symmetric case with the region of vorticity at the left thigh wrapping down into the lower wake. In the symmetric–symmetric case, the region of vorticity at the right thigh extends down towards the right foot. This behaviour is due to the change in the vortices at the feet. In the symmetric–symmetric case, there is a strong positive vortex on the outside of the right foot. This results in a broad region of vorticity banding between the thigh and foot. However, in the asymmetric–symmetric case the positive right heal vortex is absent. In contrast, there is the additional negative vortex at the left foot and a band of vorticity is observed between the thigh and heel.

4.3 Symmetric–asymmetric condition

Potential changes to the asymmetric regime of a trailing cyclist were investigated by having the asymmetric cyclist model positioned behind the symmetric cyclist. Vorticity results for this case are shown in Fig. 7g, h. As with the asymmetric–symmetric condition, the wake behind the trailing asymmetric cyclist remains very similar to the case of the single asymmetric cyclist. However, compared to the single cyclist profile, the primary hip vortex pair is reduced

Fig. 8 Streamwise velocity contours immediately downstream of: **a** a single cyclist in the symmetric condition, **b** the leading cyclist in Spacing 1 (symmetric–symmetric), and **c** leading cyclist in Spacing 2 (symmetric–symmetric)
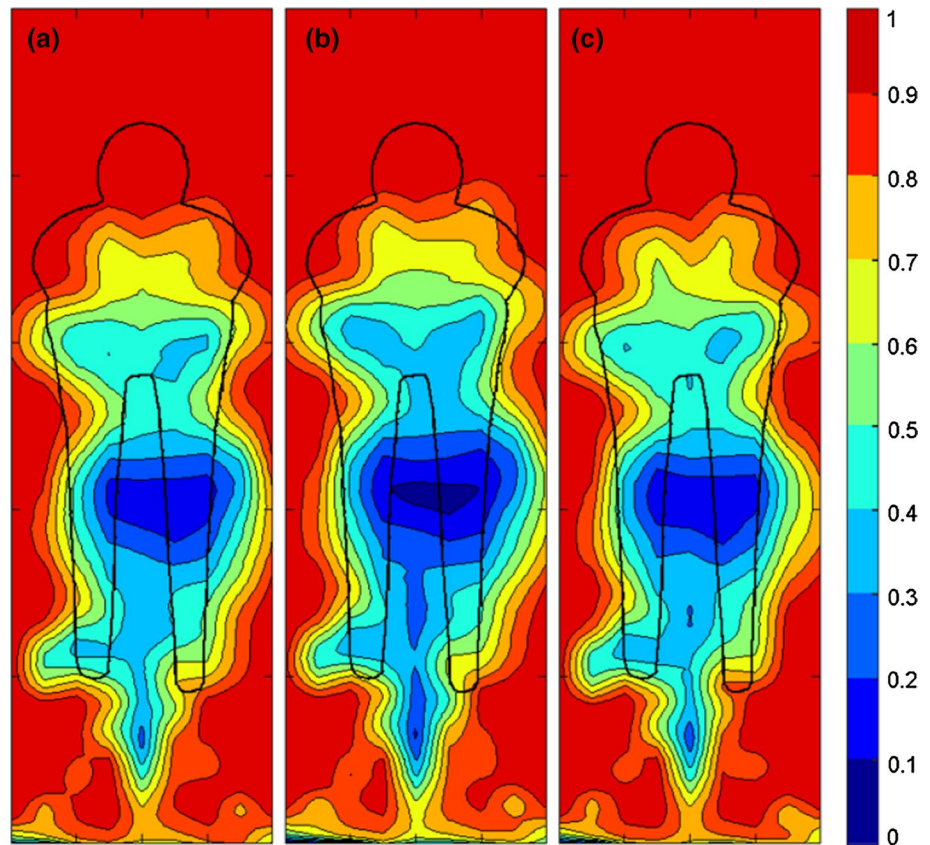
in size and vorticity, but remains the dominant feature of the wake for both Spacing 1 and Spacing 2.

At Spacing 1, the peak vorticity of the hip vortices is reduced by 41 and 27%, respectively. The degree of cross-flow between the two hip vortices is also reduced compared to the single cyclist case. The knee vortex has diffused and has moved lower and wider in the wake, with a 52% reduction in peak vorticity compared to the single cyclist condition for Spacing 1. This behaviour is similar to the movement of the thigh vortices seen in the symmetric wake cases at Spacing 1 and likely due to the reduced energy inflow conditions and cross-flow components and vorticity in the inflow affecting formation and evolution of structures in the trailing condition. The small features in the lower region of the wake are not evident in the trailing cyclist wake. This can be attributed to disruption to their formation by the upstream flow and cross-annihilation with vorticity from the leading cyclist's wake. A negative vortex shed from the right foot is still evident as is a small positive region behind the left foot.

The increased distance between the leading and the trailing cyclists in Spacing 2 has little effect on the global structure of the wake. The primary counter-rotating hip vortex pair is similar to that for Spacing 1 and of reduced strength compared with the single cyclist result. Peak vorticity is reduced by 32 and 26% compared to the single cyclist result, which represents a small increase in vorticity compared to Spacing

1. The lower section of the wake is also similar to Spacing 1, with small structures from the single cyclist case no longer evident, showing greater diffusion and cross-annihilation.

5 Flow between two tandem cyclists

### 5.1 Lead cyclist wake (asymmetric–asymmetric condition)

The wake cross sections showed that the primary longitudinal vortex structures are not significantly altered for trailing cyclists at both spacings. These changes do not appear sufficient to explain the significant drag reduction observed for a trailing cyclist, being up to 49% at minimum separation (Spacing 1) and still up to 34% with a bicycle length gap (Spacing 2). Therefore, this drag reduction must be the result of an additional mechanism upstream of the cyclist. To investigate this, flow cross sections were generated in the region between the leading and trailing cyclists for both Spacing 1 and 2. In all cases discussed in this section, the cyclists were at the symmetric leg position. Figure 8 shows the normalised streamwise velocity contours immediately downstream of the leading cyclist's rear wheel for each of the three cases. Due to the presence of the trailing cyclist, any cross sections viewed further downstream would cut

through the trailing cyclist model and therefore include physical blockage and shadowing. At Spacing 1, there is only a very narrow region where the image is not obscured and a full cross section can be viewed. In all cases, the near wake has closed at this point and no mean negative streamwise velocity is observed. However, some recirculating flow (negative streamwise velocity) is present forward of the trailing edge of the cyclist's rear wheel, behind the buttocks. This can be seen by velocity contours provided in Figure S4 of the supplementary online material; these show the mean velocity field in the X–Z plane and highlight the downwash induced in the lead cyclist's wake.

It can be seen that the three fields are all very similar in shape and magnitude. Considering Fig. 8a, c, corresponding to the single cyclist and to Spacing 2, respectively, the two streamwise velocity fields exhibit minimal difference. This indicates that the trailing cyclist has limited forward influence on the leading cyclist at this separation distance. This is consistent with previous observations in drag that show negligible change in force for the leading cyclist with a second cyclist at Spacing 2 (one bicycle length separation). Figure 8b shows the velocity behind the tandem leader at Spacing 1 and shows a slight difference from the other two fields. There is an increase in the velocity deficit, predominantly in the centre of the wake, compared to the single or Spacing 2 cases.

These velocity effects can be quantified by averaging the velocity over the whole field. Normalised velocity for the single cyclist, tandem cyclists at Spacing 1 and Spacing 2 were 0.76, 0.73 and 0.76, respectively. This confirms that the overall velocity difference between the single cyclist and the leader at Spacing 2 is negligible. However, at Spacing 1 the velocity deficit across the leader is greater than for a single cyclist despite having lower drag. Therefore, other mechanisms must cause the difference.

The velocity defect for Spacing 2 is consistent with force results, which have reported negligible drag reduction for similar cyclist separation, indicating that the lead cyclist is beyond the range of forward interference effects from the trailing cyclist. However, at Spacing 1 a drag reduction in the order of 2–5% has been reported for the lead cyclist. The mean velocity cross section results show a decrease in velocity, which indicates a greater energy loss compared to the single cyclist, suggesting an increase in drag. In fact, the reduced velocity is likely to be a result of forward interference from the trailing cyclist, as this plane is immediately upstream of the trailing cyclist leading edge. Numerical simulations by Blocken et al. (2013) showed that the presence of the trailing cyclist acted to increase the pressure on the rear surface of the leading cyclist, and it is this effect that is responsible for the leading cyclist drag reduction. However, pressure data were not derived from the flow measurements undertaken in this study.
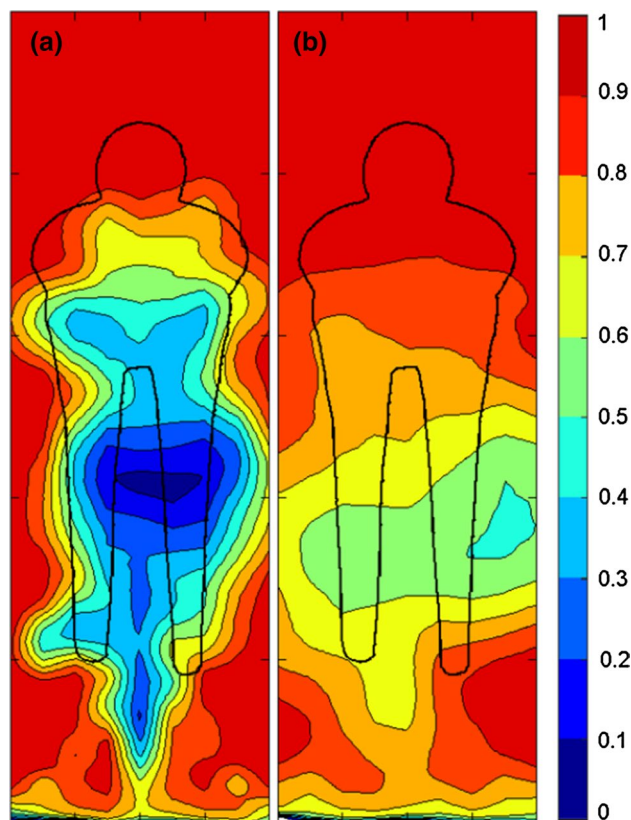
Fig. 9 Streamwise velocity immediately upstream of the trailing cyclist for the symmetric–symmetric case at Spacing 1 (**a**), and Spacing 2 (**b**)

5.2 Trailing cyclist inflow conditions

From the preceding discussion, it is suggested that the primary mechanism for drag reduction for a trailing cyclist is due to large changes in inflow velocity, rather than significant disruption to the flow structures in the wake. Figure 9 shows the streamwise velocity profiles immediately ahead of the trailing cyclist for Spacing 1 and 2.

Inflow conditions for the two cases differ significantly, as was expected given the significant change in separation distance. With the trailing cyclist positioned further downstream at Spacing 2 (Fig. 9b), there is greater distance for mixing and energy recovery in the wake. This is evident from the higher streamwise velocity across the field. Whilst there is still a large region where the velocity is well below freestream conditions, the upper wake region shows substantial recovery, approaching freestream conditions.

To quantitatively compare the state of the flow at the inlet and outlet for each configuration, the streamwise velocity component was averaged over the full cross-sectional planes at the leading and trailing edges for each bicycle. The cross-sectional region used for averaging will affect the computed averages, so this is only useful as a

Table 1 Square of the mean normalised streamwise velocity averaged over flow cross sections

	Mean inflow	Mean outflow	Velocity deficit	Reduction inflow	Drag reduction
Single cyclist	1.00	0.60	0.40	n/a	n/a
Spacing 1					
Lead	1.00	0.55	0.45	0	5%[b]
Trail	0.55	0.52	0.03	45%	49%[b]
Spacing 2					
Lead	1.00	0.59	0.41	0	0
Trail	0.67	0.52–0.60[a]	0.15–0.07[a]	33%	34%[c]

[a] Trailing cyclist wake at Spacing 2 was outside interrogation region-modelled as worst case

[b] Barry et al. (2014a, b)

[c] Barry (2016)

comparison between the different cases. The square of the mean velocity is tabulated as it provides an indication of the dynamic pressure at inlet and outlet for each case (Table 1). Drag reductions for tandem cyclists from a wind tunnel are also presented for reference (Barry et al. 2014a, b; Barry 2016).

The trailing cyclist outflow for Spacing 2 was outside the interrogation region. Given the similarity of the trailing cyclist wake at Spacing 2 to the single cyclist case, it is estimated in Table 1 to be between that of a single cyclist and the trailing outflow result for Spacing 1. The trailing cyclist at Spacing 1 has the lowest mean velocity outflow so this represents a conservative case in terms of local velocity deficit over the cyclist at Spacing 2. However, it is seen that the resulting deficit is still significantly lower than that seen for the leading or single cyclist cases due to the reduction in inflow velocity.

It can be seen that the inflow conditions vary far greater than those at outflow. This is unsurprising given the similarity observed in the vorticity cross sections of the wake. The area-averaged inflow for the trailing cyclists at Spacing 1 and Spacing 2 was 0.55 and 0.67, respectively. For comparison, the leading cyclist outflow in Spacing 2 was 0.59, close to that of a single cyclist in isolation. This shows that at greater downstream distance the flow recovers some energy from the freestream. This is consistent with drag results from wind tunnel tests, which have shown that drag reduction for the trailing cyclist decreases with distance downstream.

At minimum separation, the trailing cyclist has a lower mean outflow (0.52) than that for a single cyclist (0.60). However, the trailing cyclist has been previously shown to experience a large drag reduction. This indicates that it is not a recovery of streamwise energy in the wake that is responsible for the large drag reduction, but rather an upstream effect, as the trailing cyclist inflow velocity is significantly below freestream. This results in a significant change in the velocity deficit over the cyclist. This supports the contention that it is the reduction in inflow velocity

that is the primary contributor to the trailing cyclist drag reduction.

Results in Table 1 show that the percentage reduction in squared velocity at the inflow is of similar order to the drag saving observed for trailing cyclists in the wind tunnel. This provides quantitative evidence that the drag of the trailing cyclist is dominated by the reduction in inflow energy, rather than a downstream effect. It is noted that the trailing cyclist was observed to have lower mean velocity in the wake than a single cyclist, suggesting that drag reduction will not be directly proportional to reduction in inlet dynamic pressure. Furthermore, vorticity results showed lower magnitude of streamwise vorticity in the trailing cyclist wake. However, these effects appear to be secondary contributors to the trailing cyclist drag saving behind the reduction in inlet momentum.

5.3 Normalised streamwise vorticity

To investigate the influence of inflow energy on the wake structure of the trailing cyclist, the trailing cyclist velocity fields were corrected for a lower inlet velocity. The mean value of streamwise velocity was calculated from the streamwise cross section fields ahead of the trailing cyclist (as shown in Fig. 9; Table 1). Velocity fields were then normalised by these local values, rather than freestream velocity and streamwise vorticity recalculated from the new velocity fields. To quantitatively compare the magnitude of vorticity between the cases, the peak (positive and negative) vorticity was calculated for each of the identified hip and thigh vortices in both the symmetric and asymmetric wake cases. Peak values were calculated within the vortex boundary area identified using the swirling strength criterion.

The resulting values of peak vorticity for the hip and thigh vortices for each of the wake profiles are presented in Table 2. Only hip vortices are shown in the asymmetric case as thigh vortices are no longer distinct at that leg position. As the inlet velocity for the trailing cyclist was only measured for the symmetric–symmetric case, the

Table 2 Peak vorticity magnitude in the primary vortices in the wake of a symmetric cyclist

		Left hip		Right hip		Left thigh		Right thigh	
		Raw	Norm	Raw	Norm	Raw	Norm	Raw	Norm
Single	Symmetric	−4.5	−4.5	4.9	4.9	−3.3	−3.3	3.8	3.8
Spacing 1	Sym–sym	−3.3	−4.6	3.5	4.8	−1.6	−2.2	2.1	2.8
Spacing 2	Sym–sym	−3.3	−4.01	3.7	4.6	−1.9	−2.4	2.7	3.4
Spacing 1	Asym–sym	−3.5	−4.7	3.1	4.3	−2.3	−3.2	1.6	2.2
Spacing 2	Asym–sym	−4.0	−5.0	3.8	4.8	−2.5	−3.1	1.6	2.0
Single	Asymmetric	−8.0	−8.0	5.5	5.5				
Spacing 1	Sym–asym	−4.7	−6.5	4.0	5.5				
Spacing 2	Sym–asym	−5.4	−6.8	3.8	4.7				

Values taken within vortex boundaries identified from swirling strength criterion. 'Norm' refers to normalised vorticity, calculated from in-plane velocity fields normalised by trailing cyclist inflow velocity rather than freestream

same value of inlet was used for all cases. Although this is a simplification, the velocity values will be of the correct order compared to freestream, and so provides a reasonable model for indicative trends in the vorticity.

In the symmetric cases, it can be seen that for the four identified vortices (left and right, hip and thigh), normalising the vorticity has resulted in an increase in both peak and mean vorticity. In the case of the hip vortices, normalising the inlet velocity has corrected the vorticity to be of the same order as the single cyclist result, on both the left and right. This suggests that the reduction in streamwise velocity at the inlet for the trailing cyclist accounts for a large portion of the loss in vorticity identified in the trailing cyclist hip vortices. However, in the case of the thigh vortices, the maximum and mean vorticity does not recover to the same level as the single cyclist wake. This indicates that there are other factors influencing the vorticity in addition to the reduction in streamwise velocity.

Results have shown that the flow approaching the trailing cyclist's legs is not only reduced in streamwise velocity but also contains vorticity and in-plane velocity components from the leader wake. Given that the inner thigh vortices are formed from flow separating on the inside of the legs, the combined effect of these changes will alter the formation and evolution of the thigh vortices which results in the complex changes observed in vorticity profiles, noting that spatial distribution of the thigh vortices varies as well as peak and mean vorticity. By comparison, the hip vortices result from interaction between flow over the hip and flow down the back. *XZ* centreline planes have shown that the flow down the back of the trailing cyclist is not significantly different from the single cyclist case. This results in smaller disruption to the hip vortices. The fact that vorticity calculated from locally normalised velocity fields is of similar order to the single cyclist wake shows that the streamwise losses are the main mechanism responsible for the reduced vorticity in the dominant hip vortices in the trailing cyclist wake.

In the asymmetric cases, the wake is dominated by the hip vortices, with thigh vortices no longer distinct structures. As such, only the left and right hip vortices are identified in this analysis. Normalising vorticity shows a recovery in peak vorticity in the left vortex. However, a full recovery is not evident at either Spacing 1 or 2. This indicates that the reduction in streamwise velocity alone cannot account for the losses in the wake, and there is some influence from the disturbances in the inflow due to the lead cyclist. In contrast, the right hip vortex shows recovery of normalised vorticity closer to the single cyclist values, indicating that inlet energy accounts for much of the losses observed in the trailing cyclist wake.

The normalisation of velocity fields by local inlet velocity is approximate as a constant mean reduction was used and consideration of in-plane velocity components was not considered. However, the significant recovery of vorticity in the dominant hip vortices shows that a large portion of the reduction in vorticity seen in the trailing cyclist wake is attributable to the reduction in inlet energy for the trailing cyclist in a tandem pair.

6 Conclusion

Profiles of streamwise vorticity in the wake of tandem cyclists have shown that the flow structure in the wake of a trailing cyclist maintains similarity with that observed for a single cyclist. This is apparent for both symmetric and asymmetric conditions. The largest difference in the wake of trailing cyclist was for the smallest spacing (Spacing 1) for both a symmetric and asymmetric leading cyclist. Hip vortices remain the dominant wake structures. Here, however, they are displaced downwards due to the increased negative vertical velocity in the oncoming flow due to the wake of the leader. The thigh vortices in the symmetric case were displaced downwards and away from the centreline,

which is suggested to be the result of changes to the flow between the cyclist's legs. As separation was increased, the wake profile more closely resembles the single cyclist distribution due to reduction in in-plane velocity components and coherence of vortices from the leader's wake. In the symmetric trailing cyclist case, the thigh vortices exhibit a significant reduction in vorticity and at Spacing 1 and are displaced away from the centreline. A complex shape upstream with asymmetric wake does not significantly affect the downstream structures.

Analysis of the streamwise velocity at the inlet and outlet of each cyclist has shown that the velocity deficit over the trailing cyclist is significantly smaller than a single or leading cyclist. The magnitude of vorticity behind a trailing cyclist is reduced compared to the single cyclist case; however, by normalising the vorticity fields by local inlet velocity, rather than freestream, a significant increase in peak and mean vorticity was observed relative to the freestream case. Whilst normalised vorticity in the hip vortices was close to the single cyclist case, the thigh vortices remain lower magnitude, indicating dependence on more than just inlet streamwise velocity. As distance between the leader and trailing cyclist increases, energy is recovered from the freestream, increasing the effective inflow velocity for the trailing cyclist and thus the drag saving is diminished. Therefore, the reduction in streamwise momentum at the inlet is the major contributor to the drag reduction observed for a trailing cyclist.

The Reynolds number at which experiments were conducted is an order of magnitude lower than experienced by a real world cyclist. However, comparison with full-scale results shows a surprisingly similar flow topology; however, a higher rate of diffusion of longitudinal vortex structures is evident. We believe the implication is that separation distances we tested at scale are representative of larger spacings than the equivalent full-scale spacing. As a corollary, the interaction effects identified, such as the displacement of the thigh vortices for the symmetric case of a trailing cyclist at small separation, are likely to be more pronounced at full scale than we have observed in these experiments.

References

Barry N (2016) Aerodynamic interactions between multiple cyclists. Ph.D. thesis. Monash U, Clayton. Monash University Research Repository

Barry N, Burton D, Sheridan J, Brown NAT (2014a) The effect of spatial position on the aerodynamic interactions between cyclists. Proced Eng 72:774–779. doi:10.1016/j.proeng.2014.06.131

Barry N, Burton D, Sheridan J, Brown NAT (2014b) Aerodynamic performance and riding posture in road cycling and triathlon. Proc Inst Mech P J Sports Eng Technol. doi:10.1177/1754337114549876

Barry N, Burton D, Sheridan J, Thompson M, Brown NAT (2015) Aerodynamic drag interactions between cyclists in a team pursuit. Sports Eng 18:93–103. doi:10.1007/s12283-015-0172-8

Biermann D, Herrnstein WH Jr (1933) The interference between struts in various combinations. Report National Advisory Committee for Aeronautics, Report No. 468

Blocken B, Defraeye T, Koninckx E, Carmeliet J, Hespel P (2013) CFD simulations of the aerodynamic drag of two drafting cyclists. Comput Fluids 71:435–445. doi:10.1016/j.compfluid.2012.11.012

Blocken B, Toparlar Y, Andrianne T (2016) Aerodynamic benefit for a cyclist by a following motorcycle. J Wind Eng Ind Aerodyn 155:1–10. doi:10.1016/j.jweia.2016.04.008

Crouch TN, Sheridan J, Burton D, Thompson M, Brown NAT (2012) A quasi-static investigation of the effect of leg position on cyclist aerodynamic drag. Proced Eng 34:3–8. doi:10.1016/j.proeng.2012.04.002

Crouch TN, Burton D, Brown NAT, Thompson MC, Sheridan J (2014) Flow topology in the wake of a cyclist and its effect on aerodynamic drag. J Fluid Mech 748:5–35. doi:10.1017/jfm.2013.678

Crouch TN, Burton D, Thompson MC, Brown NAT, Sheridan J (2016) Dynamic leg-motion and its effect on the aerodynamic performance of cyclists. J Fluids Struct 65:121–137. doi:10.1016/j.jfluidstructs.2016.05.007

Defraeye T, Blocken B, Koninckx E, Hespel P, Verboven P, Nicolai B, Carmeliet J (2014) Cyclist drag in team pursuit: influence of cyclist sequence, stature, and arm spacing. J Biomech Eng 136(1):011005

Deng J, Ren A-L, Zou J-F, Shao X-M (2006) Three-dimensional flow around two circular cylinders in tandem arrangement. Fluid Dyn Res 38(6):386–404. doi:10.1016/j.fluiddyn.2006.02.003

Edwards AG, Byrnes WC (2007) Aerodynamic characteristics as determinants of the drafting effect in cycling. Med Sci Sport Exerc. doi:10.1249/01.mss.0000239400.85955.12

Fouras A, Soria J (1998) Accuracy of out-of-plane vorticity measurements derived from in-plane velocity field data. Exp Fluids 25:409. doi:10.1007/s003480050248

Fouras A, Lo Jacono D, Hourigan K (2008) Target-free stereo PIV: a novel technique with inherent error estimation and improved accuracy. Exp Fluids 44:317–329. doi:10.1007/s00348-007-0404-1

García-López J, Rodríguez-Marroyo JA, Juneau C-E, Peleterio J, Martínez AC, Villa JG (2008) Reference values and improvement of aerodynamic drag in professional cyclists. J Sports Sci 26(3):277–286

Gibertini G, Grassi D (2008) Cycling aerodynamics. Sport Aerodyn 506:23–47. doi:10.1007/978-3-211-89297-8_3

Grappe F, Candau R, Bello A, Rouillon JD (1997) Aerodynamic drag in field cycling with special reference to the Obree's position. Ergonomics 40(12):1299–1311

Griffith MD, Crouch T, Thompson MC, Burton D, Sheridan J, Brown NAT (2013) Computational fluid dynamics study of the effect of leg position on cyclist aerodynamic drag. J Fluids Eng. doi:10.1115/1.4027428

Hammache M, Michaelian M, Browand F (2002) Aerodynamic forces on truck models, including two trucks in tandem. SAE Technical Paper 2002-01-0530. doi:10.4271/2002-01-0530

Hori E (1959) Experiments on flow around a pair of parallel circular cylinders. In: Proceedings of the 9th Japan national congress for applied mechanics. Tokyo, pp 231–234

Ioannou PA (1997) Automated highway systems. Plenum Press, New York

Ishigai S, Nishikawa E, Nishimura K, Cho K (1972) Experimental study on structure of gas flow in tube banks with tube axes normal to flow (Part 1, Karman vortex flow around two tubes at various spacings). Bull Jpn Soc Mech Eng 15(86):949–956

Kawamura TM (1953) Wind drag of bicycles. Report No. 1, Tokyo University

Kyle CR (1979) Reduction of wind resistance and power output of racing cyclists and runners travelling in groups. Ergonomics 22(4):387–397. doi:10.1080/00140137908924623

Kyle CR, Burke ER (1984) Improving the racing bicycle. Mech Eng J Am Soc Mech Eng 106:34–45

Lee T, Basu S (1997) Nonintrusive measurements of the boundary layer developing on a single and two circular cylinders. Exp Fluids 23:187–192

Lin J-C, Yang Y, Rockwell D (2002) Flow past two cylinders in tandem: instantaneous and averaged flow structure. J Fluids Struct 16(8):1059–1071. doi:10.1006/jfls.2002.0469

Olds T (1998) The mathematics of breaking away and chasing in cycling. Eur J Appl Physiol 77:492–497

Romberg GF, Chianese F Jr, Lajoie RG (1971) Aerodynamics of race cars in drafting and passing situations. SAE Technical Paper 710213. doi:10.4271/710213

Sumner D (2010) Two circular cylinders in cross-flow: a review. J Fluids Struct 26:849–899. doi:10.1016/j.jfluidstructs.2010.07.001

Torre AI, Íñiguez J (2009) Aerodynamics of a cycling team in a time trial: Does the cyclist at the front benefit? Eur J Phys 30:1365–1369

Venning J, Lo Jacono D, Burton D, Thompson M, Sheridan J (2015) The effect of aspect ratio on the wake of the Ahmed body. Exp Fluids 56(6):126. doi:10.1007/s00348-015-1996-5

Watkins S, Vino G (2008) The effect of vehicle spacing on the aerodynamics of a representative car shape. J Wind Eng Ind Aerodyn 96(6–7):1232–1239. doi:10.1016/j.jweia.2007.06.042

Westerweel J, Elsinga GE, Adrian RJ (2013) Particle image velocimetry for complex and turbulent flows. Annu Rev Fluid Mech 45:409–436

Zdravkovich MM (1977) Review: review of flow interference between two circular cylinders in various arrangements. J Fluids Eng 99(4):618–633. doi:10.1115/1.3448871

Zdravkovich MM, Pridden DL (1977) Interference between two circular cylinders; series of unexpected discontinuities. J Wind Eng Ind Aerodyn 2(3):255–270. doi:10.1016/0167-6105(77)90026-5

Zdravkovich MM, Stanhope DJ (1972) Flow pattern in the gap between two cylinder in tandem. University of Salford Internal Report, FM 5/72

Zdravkovich MM, Ashcroft MW, Chisholm SJ, Hicks N (1996) Effect of cyclist's posture and vicinity of another cyclist on aerodynamic drag. The Engineering of Sport 1, Balkerna, Rotterdam

Zhou J, Adrian RJ, Balachandar S, Kendall TM (1999) Mechanisms for generating coherent packets of hairpin vortices in channel flow. J Fluid Mech 387:353–396. doi:10.1017/S002211209900467X